1.2 Self-consistent Modeling and Simulation of Dynamics in High-power Semiconductor Lasers

Mindaugas Radziunas and Uwe Bandelow

High-power (HP) broad-area edge-emitting semiconductor lasers (BALs) are compact, cheap, and reliable devices used in many modern applications. These devices have a relatively simple geometry, see Figure 1(a), allowing efficient energy pumping through a broad electric contact on the top of the device, and they can operate at high power (tens of watts) regimes. In many applications, BALs receive delayed optical feedback from external cavities (EC), see Figure 1(b), which can be used to improve the emission properties or to couple several BALs into a single system [1, 2].

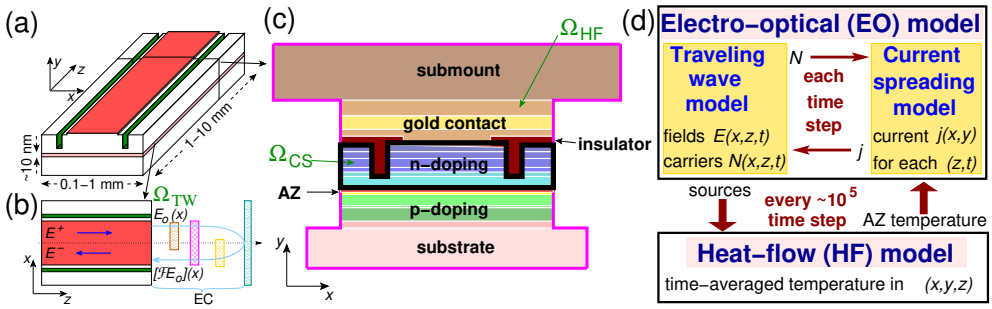

Fig. 1: *Scheme of a high-power broad-area laser (a), top view (with EC) (b), and transverse cross section with optically active zone (AZ) (c). The computational domains of model components are indicated in (b) and (c), whereas the diagram (d) illustrates the coupling of these models.*

However, operated at high power, many nonlinear processes take over, such as heating, multimode dynamics, and optical filamentation [3], [4], see Figure 2(a). As a result, the emitted optical beam is irregular, has undesirable broad optical spectra, and a large divergence. A deep understanding of the spatiotemporal dynamics in HP-BALs is needed for improving devices and novel design concepts. We model these effects at different levels of complexity [5], analyze the hierarchy of models mathematically [4], create and implement efficient and robust numerical algorithms [5, 6] into the WIAS software kit `BALaser` together with RG 3 *Numerical Mathematics and Scientific Computing*, and simulate the models typically in close collaboration with physicists and engineers in the frame of research projects [2, 3, 6].

Models, their coupling, and numerical solution strategy

Our dynamical model of HP-BALs is composed of several self-consistently coupled model components [4, 6], each operating in its own computational domain, see Figure 1(b,c,d).

Electro-optical model. The core is the traveling wave (TW) model for the envelopes E^+ and E^- of the counterpropagating optical fields, and the carrier density N within the active zone (AZ) [5]:

$$\partial_t E^{\pm} = [-i\partial_{xx} \mp \partial_z - ik_0(n_N(N) + n_T(T)) - \alpha + G(N,|E|) - \mathcal{D}]\, E^{\pm} + i\kappa E^{\mp} + F_{sp}^{\pm} \qquad (1a)$$

$$\frac{1}{\epsilon}\partial_t N = \partial_x(d_N(x,z)\partial_x N) + j(x,z) - R(N) - \Re \sum\nolimits_{\nu=\pm} E^{\nu *}\,(G - \mathcal{D})\, E^{\nu}. \qquad (1b)$$

n_N and n_T model the carrier and heat dependence of the refractive index, α, G, and $\mathcal{D}$ are the loss, the net optical gain, and its dispersion. The coupling coefficient κ accounts for the presence of Bragg gratings, and the Langevin noise term F_{sp} models spontaneous emission. In the diffusion equation for the carriers (1b), j is the injected current density, R the spontaneous recombination, and the last term the stimulated carrier recombination. At the laser facets, $z = 0$ and $z = l$, the field equations in (1a) are supplemented with reflecting-reinjecting boundary conditions:

$$E^+(x,0,t) = r_0 E^-(x,0,t), \quad E^-(x,l,t) = r_l E^+(x,l,t) + (1-|r_l|^2)[\mathcal{F}E^+(\cdot,l,\cdot)](x,t), \tag{2}$$

with reflection coefficients r_0 and r_l. The nonlocal linear operator $\mathcal{F}$ represents optical feedback, see Figure 1(b), the derivation of which for specifically designed external cavities, and its efficient numerical evaluation for dynamically varying emission is a nontrivial task by itself [1, 2].

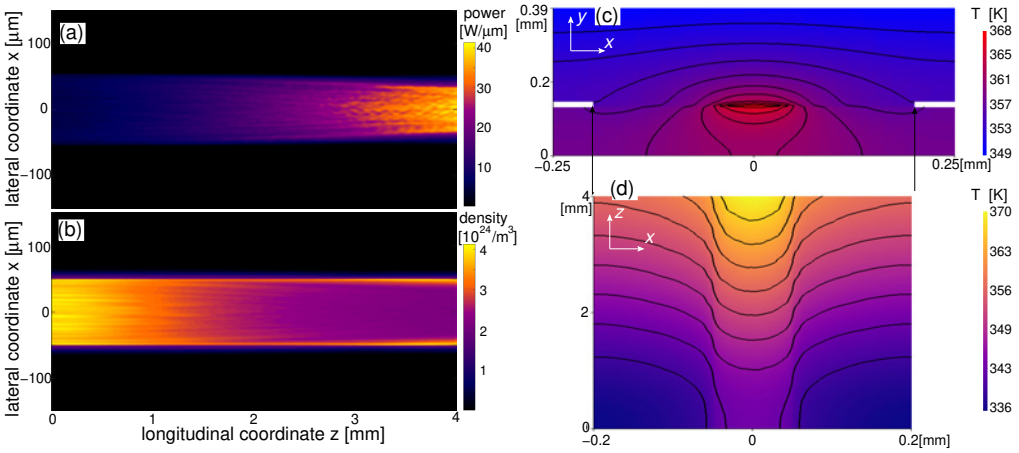

Fig. 2: *(a) and (b): Time-averaged field intensity $|E(x,z)|^2$ showing filaments, and carrier density $N(x,z)$ in the active zone, calculated by the electro-optical solver. (c) and (d): Time-averaged temperature $\bar{T}(x,y,z)$ within a transverse cross section and corresponding distribution $\bar{T}_{AZ}(x,z)$ along the active zone, provided by the heat-flow solver.*

The traveling wave model (1), (2) was extensively used for the analysis of BAL devices over the last decade, where it provided information on the main characteristics of the emission and details on the internal field and carrier distributions, Figure 2(a),(b)[1]. It is the computationally most demanding part of the coupled model; see Figure 1(d). The numerical method relies on finite differences and a split-step method for the field equations. The algorithm was parallelized using a distributed-memory paradigm. Depending on the domain's size, discretization, and the number of parallel processes, typical calculations take between a few minutes up to several hours for 1-ns long transients [5].

Simultaneously with the traveling wave model (1), (2), we calculate the current spreading (CS) in multiple cross-sections Ω_{CS} of the BAL, see thick-black framed domain in Figure 1(c) [3]:

$$\nabla_{x,y} \cdot \big(\sigma(x,y;z)\nabla_{x,y}\varphi(x,y)\big) = 0, \quad \forall z \in (0,l), \quad (x,y) \in \Omega_{\mathrm{CS}}. \tag{3}$$

The electrical conductivity σ together with the calculated Fermi potential φ define the injection current density j and diffusion d_N that enter (1b). Together with the traveling wave model, the current spreading problem (3) completes the electro-optical (EO) model, see Figure 1(d). When treating (3), we exploit finite volume schemes and the WIAS software toolkit pdelib The traveling

[1] On this level, thermal effects have been included only by a static, z-independent function $n_T(x)$ [5].

wave equations and current spreading problem solvers should exchange data during each time iteration. For the acceleration of calculations, we precalculate elementary solutions, use the current spreading problem's linearity and a Green-function-like approach [6].

Heat flow model. Due to the significant heating of the devices, we have extended the EO model above by a heat-flow (HF) model, which replaces earlier considered static contributions to the refractive index [5] by self-consistent heating-induced corrections of several parameters of the EO model. Instead of solving the classical macroscopic (1+3)-D heat-flow equation, we decompose the temperature distribution $T = \bar{T} + \Delta_T(t)$ and heat generation rate $h = \bar{h} + \Delta_h(t)$ in a time-average mean and a time-fluctuating part with zero average. With further approximations [4], the dynamic heat-flow equation splits into

$$\begin{aligned} c_h(x,y,z)\frac{\partial \Delta_T(x,y,z,t)}{\partial t} &= \Delta_h(x,y,z,t) \\ \nabla_{x,y}\cdot\big(\kappa_L(x,y;z)\nabla_{x,y}\bar{T}(x,y;z)\big) &= -\bar{h}(x,y;z) \end{aligned}, \quad \forall z\in(0,l), \quad (x,y)\in\Omega_{\mathrm{HF}}. \tag{4}$$

The first equation represents sub-ns scale fluctuations of the temperature, which can be important in high-power or in pulsed injection regimes [4]. The second equation in (4) is involved in data exchange between the EO and HF solvers, see Figure 1(d), giving the time-averaged three-dimensional distribution $\bar{T}(x,y,z)$, Figure 2(c), which has to be updated according to changes of the heat sources, typically on the ns-scale. After averaging, we obtain the mean temperature $\bar{T}_{AZ}(x,z)$ in the active zone, Figure 2(d), needed to update the EO model parameters consistently. The heat sources on the right-hand side of this equation, Figure 2(a),(b), are obtained in preceding calculations with the EO solver. For the numerical solution of this problem, we use finite-volume schemes and the pdelib toolkit [6]. For typical lasers, the calculation time required by the HF solver does not exceed a few minutes and, usually, is much smaller than the time required by the EO solver.

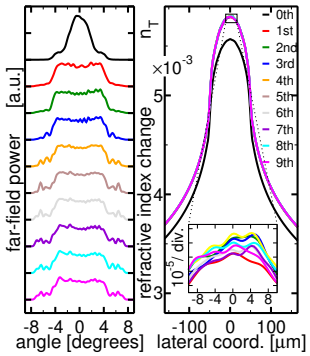

Fig. 3: *Far fields (left) and thermal corrections to the refractive index at the facet (right) during iterations of EO and HF solvers*

The EO and HF solvers are self-consistently coupled using the iterative procedure [6]. From initial transient calculations with the dynamic EO solver, time-averaged heat source distributions are obtained. Next, with these heat sources the static HF problem is solved. From the resulting temperature profile, the parameters of the EO problem are updated, in particular, the thermally induced index distribution, for the next step in this iteration. Usually, the algorithm converges already after a few iterations, see Figure 3. There, time-averaged far-field distributions are displayed on the left, corresponding refractive index profiles on the right, obtained for subsequent iteration steps. Initially, the temperature is constant, resulting in unrealistic narrow far fields (top black curve). The second iteration provides already a quite realistic far field and corrected profile of n_T. The following iterations change the far fields only little around $\pm 6^\circ$ as well as n_T (see inset of the right panel). After approximately the seventh iteration (35 ns transient simulations after switching on the laser), no more significant changes can be observed.

Example: Beam combining by a filtering external cavity

Below, we present a brightness- and power-scalable polarization beam-combining setup for HP-BALs. To achieve a beam combination, which preserves spectral, angular, and spatial characteristics of the individual emitters, we exploit Lyot-filtered optical reinjection from an external cavity. It forces the diodes to emit on interleaved frequency combs with overlapping envelopes and en-

ables a high optical coupling efficiency. Repeatedly introduced new stages of the external cavity, see Figure 4, allow efficient coupling of 2^n emitters. Properly arranged polarization beam splitters and birefringent crystals form Lyot filters, which exploit an interplay of orthogonally polarized field components and provide wavelength-periodic filtering of the propagating fields.

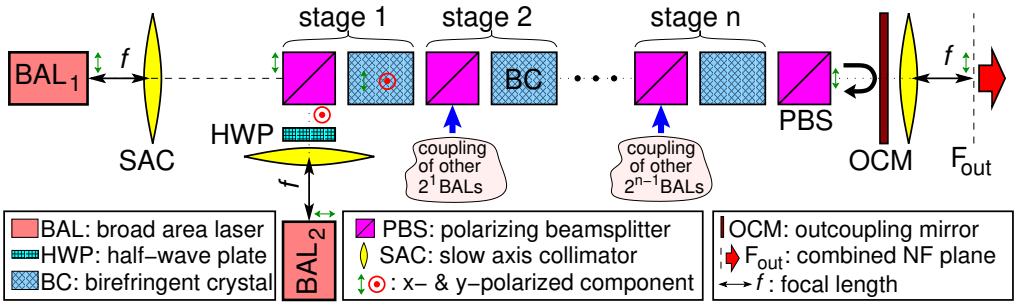

Fig. 4: *Coupling of 2^n emitters by an n-staged cascaded external cavity containing various properly located optical elements. The coupling of the first two diodes within Stage 1 is shown explicitly.*

The external cavity causes differently filtered optical re-injections $\mathcal{F}_j E^+$ to each emitter BAL $_j$, which can be incorporated into the traveling wave model by specific boundary conditions (2):

$$[\mathcal{F}_j E^+(\cdot,l,\cdot)](x,t) = \sum_{k=1}^{2^n} [M_{[j,k]} E_k^+(\cdot,l,\cdot)](x,t).$$

Operators $M_{[j,k]}$ transfer the emission of BAL $_k$ to BAL $_j$. The combined beam behind the outcoupling mirror at the plane F_{out}, see Figure 4, is a sum of 2^n fields E_k^c, which are emissions of individual diodes translated along the external cavity, $E_k^c(x,t) = [M_{[k]} E_k^+(\cdot,l,\cdot)](x,t)$, by means of operators $M_{[k]}$. For properly constructed external cavities, $M_{[j,k]}$ and $M_{[k]}$ are sums of several telescope-type operators, each introducing a different time delay, a phase shift, and a coordinate swap [1, 2]. Being local in time and space, the translation operators could be efficiently integrated into our solver.

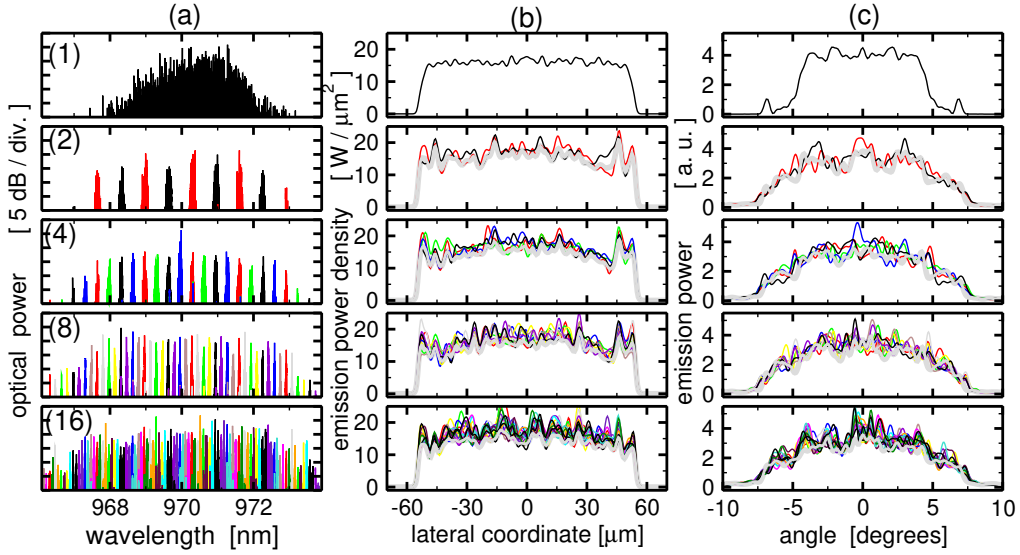

Fig. 5: *Simulations of a single diode without feedback (1) and 2/4/8/16 coupled BALs (corresponding lower rows). Optical spectra (a), near-field intensities of the individual diode emission at their front facets (b), as well as corresponding far-field distributions (c). The combined beam (divided by the number of emitters) behind the outcoupling mirror is indicated by the thick grey line in (b) and (c).*

We have simulated a single and 2/4/8/16 coupled diodes, each emitting ~ 12 W [2]. Individual interleaving optical spectra, near- and far-field distributions, as well as (scaled) combined beams of

these laser configurations are shown in Figure 5. The coupling scheme induces only a slight broadening of the spectral, spatial, and angular characteristics of the combined beam, compared to the single BAL characteristics (upper diagrams in Figure 5). The combined beam power up-scales with the number of diodes and is proportional to the coupling efficiency, which was 92.7, 89.3, 88.8, and 86.5% for 2, 4, 8, and 16 coupled BALs. The efficiencies calculated for idealized lossless external cavities are well above those of 75–80% reported for two coupled laser bars in experiments [2]. We have repeated simulations introducing 4% intensity loss within each coupling stage. The efficiency dropped to 89% and 72% in two- and sixteen-coupled-diode cases, respectively. Thus, minimization of the field losses in the external cavities is a big demand for the design of such systems.

Conclusions and outlook

We reported on a self-consistent model and software that simulates spatial-temporal dynamics in high-power broad-area edge-emitting semiconductor lasers under the impact of optical feedback and self-heating effects. The current spreading and the heat-flow models have been developed in close collaboration with our partners from Ferdinand Braun Institute, Berlin, in the frame of the BMBF-EffiLas projects. Our modeling and software tool was successfully used to optimize existing lasers and design novel high-power laser setups. For example, our modeling, simulations, and analysis performed in the frame of Eurostars project HIP-Lasers have identified the main challenge arising during the construction of cascaded beam-combining schemes of 2^n emitters, which is the minimization of field losses at the optical elements within the external cavity.

References

[1] M. Radziunas, J. Montiel-Ponsoda, G. Garre-Werner, V. Raab, *Simulation of cascaded polarization-coupled systems of broad-area semiconductor lasers*, in: Proc. 20th Int. Conf. on Numerical Simulation of Optoelectronic Devices — NUSOD 2020, J. Piprek, K. Hinzer, eds., IEEE Conf. Publ. Management Group, Piscataway, 2020, pp. 97–98.

[2] C. Bree, V. Raab, J. Montiel-Ponsoda, G. Garre-Werner, K. Staliunas, U. Bandelow, M. Radziunas, *Beam-combining scheme of high-power broad-area semiconductor lasers with Lyot-filtered reinjection: Modeling, simulations, and experiments*, J. Opt. Soc. Amer. B Opt. Phys., **36** (2019), pp. 1721–1730.

[3] A. Zeghuzi, M. Radziunas, H.-J. Wünsche, J.-P. Koester, H. Wenzel, U. Bandelow, A. Knigge, *Traveling wave analysis of non-thermal far-field blooming in high-power broad-area lasers*, IEEE J. Quantum Electron., **55** (2019), pp. 2000207/1–2000207/7.

[4] U. Bandelow, M. Radziunas, A. Zeghuzi, H.-J. Wünsche, H. Wenzel, *Dynamics in high-power diode lasers*, Proc. SPIE, Semiconductor Lasers and Laser Dynamics IX, **11356** (2020), pp. 113560W/1–113560W/14.

[5] M. Radziunas, *Modeling and simulations of broad-area edge-emitting semiconductor devices*, Int. J. High Perform. Comput. Appl., **32** (2018), pp. 512–522.

[6] M. Radziunas, J. Fuhrmann, A. Zeghuzi, H.-J. Wünsche, T. Koprucki, C. Bree, H. Wenzel, U. Bandelow, *Efficient coupling of dynamic electro-optical and heat-transport models for high-power broad-area semiconductor lasers*, Opt. Quantum Electron., **51** (2019), pp. 69/1–69/10.